HHS Public Access

Author manuscript

Am J Ophthalmol. Author manuscript; available in PMC 2019 October 01.

Published in final edited form as:

Am J Ophthalmol. 2018 October ; 194: 120–125. doi:10.1016/j.ajo.2018.07.012.

Quantitative comparison of near-infrared versus short-wave autofluorescence imaging in monitoring progression of retinitis pigmentosa

Ruben Jauregui[1,2,3], **Karen Sophia Park**[1,2], **Jimmy K. Duong**[4], **Janet R. Sparrow**[1,2,5], and **Stephen H. Tsang**[1,2,5,§]

[1]Department of Ophthalmology, New York-Presbyterian Hospital, New York, NY, USA

[2]Jonas Children's Vision Care and Bernard & Shirlee Brown Glaucoma Laboratory, New York, NY, USA

[3]Weill Cornell Medical College, NY, USA

[4]Department of Biostatistics, Columbia University, New York, NY, USA

[5]Department of Pathology & Cell Biology, Stem Cell Initiative (CSCI), Institute of Human Nutrition, College of Physicians and Surgeons, Columbia University, New York, NY, USA.

Abstract

Purpose: To quantitatively compare near-infrared autofluorescence (NIR-AF) and short-wave autofluorescence (SW-AF) as imaging modalities used to monitor retinitis pigmentosa (RP) disease progression, measured as a function of hyperautofluorescent ring constriction over time.

Design: Retrospective cohort study.

Methods: NIR-AF and SW-AF images were acquired from 22 participants (44 eyes) at two clinic visits separated by an average of 2 years. On the images from each modality, the horizontal and vertical diameters and area of the hyperautofluorescent rings were measured twice, two weeks apart. A progression rate for each parameter was obtained. Descriptive and comparative statistics were calculated to analyze these parameters and their respective progression rates.

Results: At both visits, the hyperautofluorescent ring exhibited a larger horizontal diameter (both visits: $P<0.001$), vertical diameter (visit 1: $P<0.001$, visit 2: $P=0.040$), and ring area (visit 1: $P=0.001$, visit 2: $P=0.011$) in SW-AF versus NIR-AF images. In SW- AF, the horizontal diameter, vertical diameter, and ring area decreased yearly by 168 ± 204 μm, 131 ± 159 μm, and 0.7 ± 1.1 mm^2, respectively, while in NIR-AF, they decreased by 151 ± 156 μm, 135 ± 190 μm, and 0.7

[§]Corresponding author Address Correspondence: Stephen H. Tsang, MD, PhD, Harkness Eye Institute, Columbia University Medical Center, 635 West 165th Street, Box 212, New York, NY 10032, Phone: (212) 342-1189 / Fax: 212-305-4987 / sht2@cumc.columbia.edu.

Revision statement: Each co-author has seen and agrees with each of the changes made to this manuscript in the revision and to the way his or her name is listed.

± 1.0 mm^2. No difference was observed in these rates between SW-AF and NIR-AF. Similar results were observed in the left eye.

Conclusions: In SW-AF and NIR-AF images, similar rates of RP disease progression are observed. As such, NIR-AF may confer more advantages as the primary tool for tracking disease progression over the commonly used SW-AF, given the increased patient comfort and cooperation during imaging.

Introduction

Retinitis pigmentosa (RP) refers to a group of rod-cone dystrophies characterized by early nyctalopia and progressive visual field constriction, leading to tunnel vision and eventual blindness.[1–3] Non-syndromic RP occurs in approximately 1 in 4,000 people worldwide and can be inherited in an autosomal recessive (50–60% of cases), autosomal dominant (30–40%), or X-linked (5–15%) pattern.[1] As a clinically and genetically heterogeneous disease, non-syndromic RP can be caused by more than 50 genes.[4] The primary defect lies in the rod photoreceptors, whose degeneration leads to secondary cone photoreceptor death.[2]

Two non-invasive imaging techniques are traditionally used to monitor disease progression in patients with RP: spectral domain optical coherence tomography (SD- OCT) and short-wavelength autofluorescence (SW-AF). SD-OCT is used to track decreases in ellipsoid zone (EZ) line width over time. The point at which the EZ line disappears marks the boundary between unhealthy and healthy retina, thereby corresponding to the edge of normal retinal sensitivity.[5–7] For this reason, multiple studies have relied on EZ line width as a tool for measuring RP disease progression.[8–11]

SW-AF is another classical technique that derives its signals (488 nm excitation) from retinal pigment epithelium (RPE) lipofuscin, originally formed in photoreceptors as a product of reactions involving all-*trans*-retinal.[12–15] Patients with RP often exhibit a ring of hyperautofluorescence that encircles an area of the fundus with relatively normal autofluorescence. Studies have shown that the inner border of this hyperautofluorescent ring corresponds spatially to the lateral end of the EZ line on SD-OCT.[6] Between the inner and outer borders of the ring, cone-mediated visual function is relatively preserved and the retina exhibits an intact structure and thickness.[16] In addition, studies quantifying the SW-AF signal within the ring have shown an actual increase in SW-AF intensity relative to corresponding areas in healthy retina, suggesting that lipofuscin fluorophore production increases as a part of the RP disease process.[17] As the disease progresses, the EZ line shortens over time along with a proportional constriction of the hyperautofluorescent ring, allowing SW-AF to serve as a useful imaging modality for monitoring disease progression.[8,14,16]

Though less widespread, the use of near-infrared autofluorescence (NIR-AF) has been expanding over the last several years, as multiple studies have applied this modality to RP and other diseases such as recessive Stargardt disease (STGD1) and Best vitelliform macular dystrophy.[14,18–21] The NIR-AF signal (787 nm excitation) is thought to originate mostly from melanin in the RPE with a smaller contribution from the choroid.[22] Previous studies have shown that a ring of hyperautofluorescence is also visualized in RP patients through

NIR-AF and have assessed the relationship between SW-AF and NIR-AF in RP patients.[14] In this study, we analyzed RP disease progression rates using both SW-AF and NIR-AF and, based on our findings, assess the modalities as tools for tracking disease progression.

Methods

Patients and Clinical Examination

All study procedures were defined and patient consent was obtained as outlined by the protocol #AAAR0284 approved by the Institutional Review Board at Columbia University Medical Center. The study adhered to the tenets of the Declaration of Helsinki. None of the data presented in this study, including images and genetic testing results, can be identified with individual patients. A retrospective review of 300 patients with a clinical diagnosis of retinitis pigmentosa by an inherited retinal disease specialist (SHT) was conducted at the Department of Ophthalmology at Columbia University. The clinical diagnosis was made based on presenting symptoms, family history, fundus examination, and full-field electroretinography (ffERG) and subsequently supported by clinical imaging and/or genetic testing. The inclusion criteria for this study were the diagnosis of RP along with clear media and adequate fixation to allow for high-quality imaging. In addition, each patient was screened for a history of two visits in our office at least 3 months apart consisting of a complete ophthalmic examination by a retinal physician (SHT). Ophthalmic examinations included a slit-lamp and dilated funduscopic examination, best corrected visual acuity (BCVA), SW-AF (488 nm excitation) and NIR- AF (787 nm excitation) imaging, and spectral domain optical coherence tomography (SD-OCT). The exclusion criteria precluded patients affected by any other ocular disorder or unable to fixate during the imaging procedures. Patients lacking a hyperautofluorescent ring in SW-AF or NIR-AF images were also excluded. Both the right and left eye from each patient were included in the study and analyzed separately.

Clinical Characterization

Imaging across all modalities was conducted after pupil dilation (>7 mm) with phenylephrine hydrochloride (2.5%) and tropicamide (1%). SW-AF scans (488 nm excitation) were acquired with the Spectralis HRA+OCT (Heidelberg Engineering, Heidelberg, Germany). NIR-AF scans (787 nm excitation) were acquired with the Heidelberg Retina Angiograph 2 scanning laser ophthalmoscope (HRA2-SLO) (Heidelberg Engineering, Heidelberg, Germany) using the indocyanin-green angiography mode (without injection) after adjusting the focus in near-infrared reflectance mode. The eye-tracking feature of both machines was used to obtain high- quality images with improved signal-to-noise ratio. For either modality, the scans were acquired with a field of view of 30 degrees. For larger rings that were not fully captured with the 30-degree field of view, scans with 55-degree field of view were also acquired.

Image and Statistical Analyses

Measurements of the ring area and horizontal, and vertical diameters were obtained from the SW-AF and NIR-AF scans that were acquired during the clinic visits. To mitigate bias and error in measurement of the dimensions of the hyperautofluorescent rings, the same image

from each clinic visit was analyzed twice, two weeks apart, by the first author (RJ). The measurements were performed using a built-in measurement tool in the Spectralis HRA +OCT software. The external boundary of the ring, which is better defined than the internal boundary, was used as the borderline for the diameter and area measurements. The horizontal diameter was defined as the longest distance between the nasal and temporal borders of the ring.

The statistical analyses were performed using the Stata 12.1 (StataCorp, College Station, Texas, USA) software. The Pearson correlation was calculated for the two measurements obtained two weeks apart (Table 1). Given the high correlation between the measurements, the average of the two values was calculated and used for subsequent analyses. Statistical analyses included descriptive statistics for patient demographics, follow-up time, and hyperautofluorescent ring measurements (horizontal and vertical diameters and ring area). The progression rate, defined as the difference in values obtained between the follow-up and baseline visits divided by the length of follow-up, was calculated for each measured variable. A paired Student's t-test was used to compare the averages of these variables as observed with SW-AF and NIR-AF. Due to the similarity of the results for both eyes and the bilateral symmetry of the disease, only the results for the right eye are reported.

Results

In total, 22 patients (44 eyes) were analyzed for this study and the results presented correspond to the 22 right eyes. The mean follow-up time between the two visits was 2.23 ± 1.62 years, while the mean age of presentation was 36.03 ± 16.69 years at visit 1 and 38.26 ± 16.71 years at visit 2. Demographic and genetic characterizations of the patients are summarized in Table 2.

At visit 1, the mean horizontal and vertical diameters in SW-AF images were 3135 ± 1722 μm and 2454 ± 1399 μm, respectively, while the ring area was 7.6 ± 8.6 mm^2. Measurements for these same parameters in NIR-AF images were 2952 ± 1708 μm, 2326 ± 1429 μm, and 6.9 ± 8.0 mm^2, respectively. After comparing the visit 1 measurements obtained for each parameter in SW-AF and NIR-AF images, we observed a larger ring with greater horizontal and vertical diameters in SW-AF compared to NIR-AF images ($P<0.001$ for both diameter comparisons, while $P=0.001$ for the ring area comparison). At visit 2, the mean horizontal and vertical diameters in SW-AF images were 2856 ± 1581 μm and 2221 ± 1299 μm, respectively, while the ring area was 6.3 ± 7.1 mm^2. Measurements for these same parameters in NIR-AF images were 2675 ± 1532 μm, 2127 ± 1247 μm, and 5.7 ± 6.3 mm^2, respectively. Similar to visit 1, we observed larger diameters and ring area in SW-AF as compared to NIR-AF images ($P < 0.001$, $P = 0.040$ and 0.011 for the comparisons of the horizontal diameter, vertical diameter, and ring area, respectively). These results are summarized in Table 3.

For the two visits, we also calculated the progression rates for the horizontal diameter, vertical diameter, and ring area in both SW-AF and NIR-AF. In SW-AF images, the horizontal diameter decreased at a rate of 168 ± 204 μm per year, the vertical diameter decreased at a rate of 131 ± 159 μm per year, and the ring area decreased at a rate of 0.7

± 1.1 mm^2 per year. Similar values were seen in NIR-AF images: the horizontal diameter decreased at a rate of 151 ± 156 μm per year, the vertical diameter decreased at a rate of 135 ± 190 μm, and the area decreased at a rate of 0.7 ± 1.0 mm^2. No significant difference in progression rates was calculated between the two modalities (P = 0.591, 0.877, and 0.694 for the horizontal diameter, vertical diameter, and ring area, respectively). These results are summarized in Table 3.

Discussion

In this study, both SW-AF and NIR-AF imaging revealed hyperautofluorescent rings in the macular area; these rings constricted over time as disease progressed. The dimensions of the ring, however, differed between the two AF modalities. In a previous study that also compared SW-AF and NIR-AF, the authors reported that the positions of the outer borders of rings were similar in these two modalities while the inner borders of the NIR-AF rings were closer to the fovea; these observations indicated that NIR-AF imaging may reveal smaller diameters compared to SW-AF.[14] Here, we present a more detailed, quantitative analysis of both the horizontal and vertical diameters of the hyperautofluorescent ring as well as the ring area at two different visits.

Based on measurements from both visits, we found that the NIR-AF rings were more constricted than the SW-AF rings, both in terms of the horizontal and vertical diameters and ring area. While we know that the AF signals recorded by SW-AF (lipofuscin) and NIR-AF (melanin) imaging are different, the structural and molecular features responsible for ring formation and for the differences in the ring parameters are not understood. We also used the ring measurements from both visits to calculate a progression rate for the horizontal diameter, vertical diameter, and ring area and observed no differences between the two modalities. Furthermore, we segregated our cohort of 22 RP patients into four disease subtypes (autosomal recessive RP, autosomal dominant RP, X-linked recessive RP, and Usher syndrome) to explore whether the genetics of the disease affects the progression rates between these two imaging modalities (Supplemental Table 1 available at AJO.com). We again did not observe any difference in progression rates between SW-AF and NIR-AF after segregating our initial cohort of RP patients. Some cohorts, however, particularly the X-linked recessive and Usher syndrome cohorts, contained few patients. Thus, a larger study with a greater cohort size for each mode of inheritance would serve to explore the role of mode of inheritance more accurately.

The similar progression rates between the two modalities suggest the possibility that there is an overlap of the sources that create the SW-AF and NIR-AF signals. Previous studies have indeed proposed that increased levels of RPE lipofuscin might modulate the melanin-related NIR-AF signal.[23] Although this could explain the similar progression rates observed in the two AF modalities, the difference in ring parameters measured in SW-AF and NIR-AF images would remain a question. Additional studies are needed to discern the mechanisms of ring formation in both SW-AF and NIR-AF imaging modalities in RP patients.

Although there is no current treatment available for RP, the recent emergence of multiple clinical trials for potential treatment methods, including but not limited to gene therapy, has

augmented the need for detailed characterization of RP disease progression. Traditionally, EZ line width measurements and SW-AF have commonly been used as non-invasive tools for tracking disease progression in patients with RP. However, NIR-AF, though less commonly utilized, may confer greater advantages over SW-AF. In contrast to NIR-AF, patient comfort and cooperation are diminished when they are imaged with SW-AF. While patients observe a dim, reddish light when undergoing NIR-AF scans, they experience a more intense light with SW-AF scans. Due to diminished patient comfort, the acquisition times for SW-AF scans are longer as compared to NIR-AF. These issues are of particular importance for pediatric and photophobic patients—two populations for which obtaining SW-AF scans is challenging. Furthermore, concerns have been raised about the long-term consequences of exposure to SW-AF during clinical imaging.[24] Thus, given that there appears to be no significant difference between NIR-AF and SW-AF as tools for measuring RP disease progression, NIR-AF may serve as a more efficient substitute for SW-AF in the clinic and in routine practice.

Supplementary Material

Refer to Web version on PubMed Central for supplementary material.

Acknowledgements

A. Funding/Support: This work was supported by the National Institutes of Health [P30EY019007, R01EY018213, R01EY024698, R01EY026682, R21AG050437], National Cancer Institute Core [5P30CA013696], the Research to Prevent Blindness (RPB) Physician-Scientist Award, unrestricted funds from RPB, New York, NY, USA. R.J. is supported by the RPB medical student eye research fellowship.

B. Financial Disclosures: No financial disclosures.

C. Other Acknowledgements: None

References

1. Hartong DT, Berson EL, Dryja TP. Retinitis pigmentosa. Lancet 2006;368(9549):1795–1809. [PubMed: 17113430]
2. Hamel C Retinitis pigmentosa. Orphanet J Rare Dis 2006;1:40. [PubMed: 17032466]
3. Ferrari S, Di Iorio E, Barbaro V, Ponzin D, Sorrentino FS, Parmeggiani F. Retinitis pigmentosa: genes and disease mechanisms. Curr Genomics 2011;12(4):238–249. [PubMed: 22131869]
4. Daiger SP, Sullivan LS, Bowne SJ. Genes and mutations causing retinitis pigmentosa. Clin Genet2013;84(2):132–141. [PubMed: 23701314]
5. Cai CX, Locke KG, Ramachandran R, Birch DG, Hood DC. A comparison of progressive loss of the ellipsoid zone (EZ) band in autosomal dominant and x-linked retinitis pigmentosa. Invest Ophthalmol Vis Sci 2014;55(11):7417–7422. [PubMed: 25342618]
6. Hood DC, Lazow MA, Locke KG, Greenstein VC, Birch DG. The transition zone between healthy and diseased retina in patients with retinitis pigmentosa. Invest Ophthalmol Vis Sci 2011;52(1):101–108. [PubMed: 20720228]
7. Hood DC, Ramachandran R, Holopigian K, Lazow M, Birch DG, Greenstein VC. Method for deriving visual field boundaries from OCT scans of patients with retinitis pigmentosa. Biomed Opt Express 2011;2(5):1106–1114. [PubMed: 21559123]
8. Cabral T, Sengillo JD, Duong JK, et al. Retrospective Analysis of Structural Disease Progression in Retinitis Pigmentosa Utilizing Multimodal Imaging. Sci Rep 2017;7(1):10347. [PubMed: 28871101]

9. Sujirakul T, Lin MK, Duong J, Wei Y, Lopez-Pintado S, Tsang SH. Multimodal Imaging of Central Retinal Disease Progression in a 2-Year Mean Follow-up of Retinitis Pigmentosa. Am J Ophthalmol 2015;160(4):786–798 e784. [PubMed: 26164827]
10. Birch DG, Locke KG, Wen Y, Locke KI, Hoffman DR, Hood DC. Spectral-domain optical coherence tomography measures of outer segment layer progression in patients with X-linked retinitis pigmentosa. JAMA Ophthalmol 2013;131(9):1143–1150. [PubMed: 23828615]
11. Ramachandran R, Zhou L, Locke KG, Birch DG, Hood DC. A Comparison of Methods for Tracking Progression in X-Linked Retinitis Pigmentosa Using Frequency Domain OCT. Transl Vis Sci Technol 2013;2(7):5. [PubMed: 24349883]
12. Delori FC, Dorey CK, Staurenghi G, Arend O, Goger DG, Weiter JJ. In vivo fluorescence of the ocular fundus exhibits retinal pigment epithelium lipofuscin characteristics. Invest Ophthalmol Vis Sci 1995;36(3):718–729. [PubMed: 7890502]
13. Sparrow JR, Wu Y, Kim CY, Zhou J. Phospholipid meets all-trans-retinal: the making of RPE bisretinoids. J Lipid Res 2010;51(2):247–261. [PubMed: 19666736]
14. Duncker T, Tabacaru MR, Lee W, Tsang SH, Sparrow JR, Greenstein VC. Comparison of near-infrared and short-wavelength autofluorescence in retinitis pigmentosa. Invest Ophthalmol Vis Sci 2013;54(1):585–591. [PubMed: 23287793]
15. Katz ML, Robison WG, Jr. What is lipofuscin? Defining characteristics and differentiation from other autofluorescent lysosomal storage bodies. Arch Gerontol Geriatr 2002;34(3):169–184. [PubMed: 14764321]
16. Lima LH, Cella W, Greenstein VC, et al. Structural assessment of hyperautofluorescent ring in patients with retinitis pigmentosa. Retina 2009;29(7):1025–1031. [PubMed: 19584660]
17. Schuerch K, Woods RL, Lee W, et al. Quantifying Fundus Autofluorescence in Patients With Retinitis Pigmentosa. Invest Ophthalmol Vis Sci 2017;58(3):1843–1855. [PubMed: 28358950]
18. Schuerch K, Marsiglia M, Lee W, Tsang SH, Sparrow JR. Multimodal Imaging of Disease-Associated Pigmentary Changes in Retinitis Pigmentosa. Retina 2016;36 Suppl 1:S147–S158. [PubMed: 28005673]
19. Duncker T, Marsiglia M, Lee W, et al. Correlations among near-infrared and short-wavelength autofluorescence and spectral-domain optical coherence tomography in recessive Stargardt disease. Invest Ophthalmol Vis Sci 2014;55(12):8134–8143. [PubMed: 25342616]
20. Greenstein VC, Schuman AD, Lee W, et al. Near-infrared autofluorescence: its relationship to short-wavelength autofluorescence and optical coherence tomography in recessive stargardt disease. Invest Ophthalmol Vis Sci 2015;56(5):3226–3234. [PubMed: 26024107]
21. Duncker T, Greenberg JP, Ramachandran R, et al. Quantitative fundus autofluorescence and optical coherence tomography in best vitelliform macular dystrophy. Invest Ophthalmol Vis Sci 2014;55(3):1471–1482. [PubMed: 24526438]
22. Keilhauer CN, Delori FC. Near-infrared autofluorescence imaging of the fundus: visualization of ocular melanin. Invest Ophthalmol Vis Sci 2006;47(8):3556–3564. [PubMed: 16877429]
23. Duncker T, Lee W, Tsang SH, et al. Distinct characteristics of inferonasal fundus autofluorescence patterns in stargardt disease and retinitis pigmentosa. Invest Ophthalmol Vis Sci 2013;54(10): 6820–6826. [PubMed: 24071957]
24. Cideciyan AV, Swider M, Aleman TS, et al. Reduced-illuminance autofluorescence imaging in ABCA4-associated retinal degenerations. J Opt Soc Am A Opt Image Sci Vis 2007;24(5):1457–1467. [PubMed: 17429493]

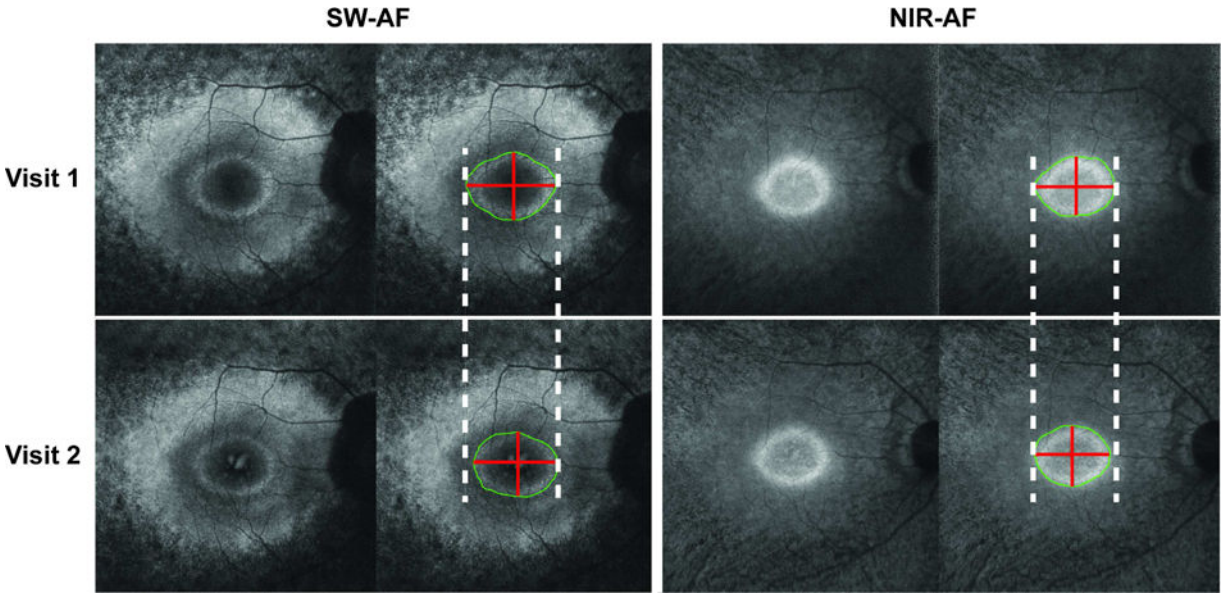

Figure. Hyperautofluorescent ring progression in short-wave vs. near-infrared autofluorescence imaging of a patient with retinitis pigmentosa.

Short-wave (SW-AF) and near-infrared autofluorescence (NIR-AF) images of a patient with autosomal dominant retinitis pigmentosa caused by the gene *KLHL7*. The left panel displays SW- AF images, while the right displays NIR-AF images. Top row images were obtained at the first visit, while those on the bottom were obtained at the follow-up visit approximately 3 years later. Dashed white lines are tangent to the horizontal-most edges of the hyperautofluorescent ring from visit 1. The outer border of the ring is outlined in green, while red lines span the length of the horizontal and vertical diameters. While both SW-AF and NIR-AF images reveal decreases in ring size over time, the difference in size is seen clearer in the SW-AF images.

Table 1.

Correlations between the repeated measurements for horizontal diameter, vertical diameter, and ring area of the hyperautofluorescent rings at visit 1 and 2.

	Horizontal diameter				Vertical diameter				Ring area			
	SW-AF		NIR-AF		SW-AF		NIR-AF		SW-AF		NIR-AF	
Pearson correlation	**Visit 1**	**Visit 2**	**Visit 1**	**Visit 2**	**Visit 1**	**Visit 2**	**Visit 1**	**Visit 2**	**Visit 1**	**Visit 2**	**Visit 1**	**Visit 2**
r	0.9995	0.9995	0.9997	0.9996	0.9993	0.9990	0.9995	0.9994	0.9996	0.9998	0.9998	0.9998
P-value	< 0.001	< 0.001	< 0.001	< 0.001	< 0.001	< 0.001	< 0.001	< 0.001	< 0.001	< 0.001	< 0.001	< 0.001

SW-AF = short-wave autofluorescence; NIR-AF = near-infrared autofluorescence; r = Pearson correlation coefficient.

Table 2.

Descriptive statistics for the demographics, genetic characterization, and follow-up time of the retinitis pigmentosa patients.

	N (%)	Age During Visit 1 (yr)			Age During Visit 2 (yr)		
Patients	22	36.03 ± 16.69			38.26 ± 16.71		
Males	13 (59.1)						
Females	9 (40.9)						
Disease subtype		**Disease-causing Gene Variants (# of patients)**					
ARRP	8 (36.3)	*CDHR1* (1), *DHDDS* (1), *MAK* (1), Unknown (5)					
ADRP	10 (45.5)	*RP1* (3), *KLHL7* (2), *PRPF31* (2), *NRL* (1), *RHO* (1), Unknown (1)					
XLRP	2 (9.1)	*RPGR* (2)					
USH	2 (9.1)	*CLRN1* (1), *USH2A* (1)					
	Mean	**Standard Deviation**	**Quantile**				
			Minimum	**25th**	**Median**	**75th**	**Maximum**
Follow-up time (yr)	2.23	1.62	0.25	0.88	1.65	3.19	5.27

Data are summarized as mean ± standard deviation where appropriate. ARRP = autosomal recessive retinitis pigmentosa; ADRP = autosomal dominant retinitis pigmentosa; XLRP = X- linked retinitis pigmentosa; USH = Usher syndrome.

Table 3.

Descriptive and statistical analyses of the horizontal diameter, vertical diameter, and ring area of the hyperautofluorescent rings observed in retinitis pigmentosa patients during visits 1 and 2, and the yearly progression rate.

	Visit 1	P-value[a]	Visit 2	P-value[a]	Progression rate per year	P-value[a]
Horizontal diameter (μm)						
SW-AF	3135 ± 1722	< 0.001	2856 ± 1581	< 0.001	− 168 ± 204	0.591
NIR-AF	2952 ± 1708		2675 ± 1532		− 151 ± 156	
Vertical diameter (μm)						
SW-AF	2454 ± 1399	< 0.001	2221 ± 1299	0.040	− 131 ± 159	0.877
NIR-AF	2326 ± 1429		2127 ± 1247		− 135 ± 190	
Ring area (mm^2)						
SW-AF	7.6 ± 8.6	0.001	6.3 ± 7.1	0.011	− 0.7 ± 1.1	0.694
NIR-AF	6.9 ± 8.0		5.7 ± 6.3		− 0.7 ± 1.0	

Data are summarized as mean ± standard deviation where appropriate. SW-AF = short-wave autofluorescence; NIR-AF = near-infrared autofluorescence.

[a]Calculated using a paired Student's t-test to test for a difference between these values.